Spotlight-mode Synthetic Aperture Radar without Fourier Transforms

Jordan Mann

Weizmann Institute of Science
Rehovot, Israel

Robert Hummel

Courant Institute of Mathematical Sciences
New York University

ABSTRACT

The spotlight mode SAR (SPSAR) image reconstruction problem may be solved using a backprojection algorithm in the spatial domain while the radar return signals being recorded. The resulting SPSAR algorithm, studied by Desai and Jenkins,[3] permits parallelization of the image reconstruction, and obviates a costly Fourier-domain resampling step. We show that by using a radar signal of a specially-designed form with backprojection, the reconstruction becomes extremely simple, eliminating the need for Fourier processing of the return signals, by incorporating a derivative of a Hilbert transform into the emitted signal. We show some simulation results using this new method. We also briefly discuss an algorithm for reconstruction of a function residing on a hemisphere from its radar returns without geometric approximation or distortion.

1 INTRODUCTION

Like computed-tomography, spotlight-mode SAR (SPSAR) involves reconstruction of a scene from its Radon transforms; that is, the reflected signal resulting from a radar "chirp" provides information about line integrals of the scene rather than information about the scene at individual points.[1,7] However, unlike computed tomography, the reconstruction method used for SAR typically involves extensive computation in the Fourier domain. Indeed, the most expensive step in conventional SAR image reconstruction involves interpolation of spectral values on a rectangular coordinate grid, given spectral values on a polar coordinate grid. Also, the Fourier domain resampling and inversion cannot begin until all radar returns have been processed.

Munson *et al.*[7] suggested that the method of backprojection, which is typically used for computer tomography (CAT) imagery reconstruction, could also be applied to SAR image formation. This suggestion has been successfully tested by Desai and Jenkins.[3] They show that using the standard chirp signal, reconstructing the Fourier data of the Radon transform of the image using the return signal, and processing that return signal with a derivative of a Hilbert transform filter, they can make use of the backprojection method to build up the reconstructed image incrementally. The advantage of the method is that the resampling in Fourier space is unnecessary, and that intermediate versions of the reconstructed image are available as the return radar chirps are processed.

In this paper, we propose an additional advance to be used in conjunction with Desai's algorithm that further reduces the time needed for image reconstruction. We propose to use a nonstandard chirp, which has built into it much of the processing that ordinarily must be done to the return radar signal. In this way, the return signal provides directly the values that are summed to form the spatial domain image. The normal processing of the Radon transform data, which consists of applying the Hilbert transform followed by a differentiation, is no longer required.

2 MATHEMATICAL CONSIDERATIONS

2.1 Classical approach

In order to formulate the reconstruction methods, let us recall that $P_\theta f(t)$, the Radon transform of the function at angle θ, is defined by

$$P_\theta f(t) = \int_{-\infty}^{\infty} f(t\cos\theta - \tau\sin\theta, t\sin\theta + \tau\cos\theta)\, d\tau. \tag{1}$$

For any particular t, $P_\theta f(t)$ is the integral of the function along a line in the coordinate plane. The Radon Slice theorem[7] states that

$$\widehat{P_\theta f}(\rho) = \sqrt{2\pi}\hat{f}(\rho\cos\theta, \rho\sin\theta), \tag{2}$$

where the "hat" indicates the normalized Fourier transform. Thus that the 2-D Fourier transform of the image can be sampled by obtaining the Fourier transform of the Radon transform for different values of θ.

We note that if a point reflector at coordinates (x, y) is at a distance l from the radar, then the time it takes the signal to travel to the reflector and back is $2l/c$, where c is the speed of light. Thus, if the transmitted signal at time t is given by $s(t)$, then the signal returning to the radar antenna from the point reflector at (x, y) at time t is given by

$$g(x, y)s(t - 2l/c),$$

where $g(x, y)$ is the reflectivity of the reflector. If the imaging region is small with respect to the distance of the imaging region from the antenna, then the set of image points lying a distance l from the antenna lie approximately on a straight line, so the integral of the reflectivity function over those points is approximately equal to $P_\theta g(l)$, where θ is the angle between a line of reference and the line connecting the antenna and the center of the imaging region. Thus the accumulated signal at time t returning from distributed reflectors at a distance l is given by

$$P_\theta g(l)s(t - 2l/c).$$

The total returning signal must be integrated over points at all distances; thus the total returning signal at time t is given by

$$r(t) = \int P_\theta g(l)\, s(t - 2l/c)\, dl.$$

Thus, with proper rescaling, the return signal is the convolution of the broadcast signal with $P_\theta g$. This implies that by dividing the Fourier transform of the return signal by that of the broadcast signal, one may obtain $\widehat{P_\theta f}$. In practice, other signal processing techniques are usually used instead.[7] $\widehat{P_\theta f}$ is sampled at discrete points, and by the Radon Slice Theorem, the values at those points are proportional to the values of the Fourier transform of the image at points on a "polar grid" in the Fourier domain (see Figure 1). Fourier transform values on nearby points on a rectangular grid must be computed by interpolation before the image can be reconstructed by inverse FFT.

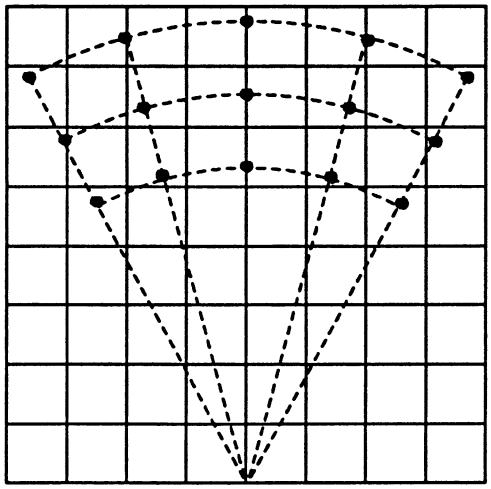

Figure 1: Fourier domain polar grid.
The samples of $\hat{g}$ obtained from the reflected signal, shown here as black dots, lie on a polar grid, shown here as dotted lines and curves. The FFT algorithm requires samples on a rectangular grid, shown here as the intersections of the solid lines.

2.2 The modified Convolution-Backprojection method

Desai[2,3] has shown that the need for interpolation in the Fourier domain can be avoided by adapting the well-known convolution-backprojection algorithm (CBP) of computed tomography for use in SPSAR. In this algorithm, it is assumed that Fourier data are known on a polar grid, and reconstruction is performed based on the following. The Fourier transform inversion formula can be written in polar coordinates as

$$g(x,y) = \frac{1}{2\pi}\int_0^\pi \int_{-\infty}^{\infty} \hat{g}(\rho\cos\theta, \rho\sin\theta)\, e^{i(x\cos\theta + y\sin\theta)}|\rho|\, d\rho\, d\theta.$$

By the Radon Slice Theorem, this equals

$$\frac{1}{(2\pi)^{3/2}}\int_0^\pi \int_{-\infty}^{\infty} \widehat{P_\theta g}(\rho)\, e^{i(x\cos\theta + y\sin\theta)}|\rho|\, d\rho\, d\theta.$$

Using the $\widehat{P_\theta g}$ values, we may compute

$$\tilde{P}_\theta g(u) = \int_{-\infty}^{\infty} \widehat{P_\theta g}(\rho)\, e^{i\rho u}|\rho|\, d\rho.$$

This is easily computed numerically by means of multiplication and inverse FFT. Thus we can see that

$$g(x,y) = \frac{1}{(2\pi)^{3/2}}\int_0^\pi \tilde{P}_\theta g(x\cos\theta + y\sin\theta)\, d\theta,$$

which means that $g(x,y)$ can be reconstructed from the $\tilde{P}_\theta$ values, given these values for all θ. In practice, pixel (x,y) simply sums $\tilde{P}_\theta g(x\cos\theta + y\sin\theta)$ for all available values of θ. This method has several advantages. It avoids interpolation in the Fourier domain. Also, the function $\tilde{P}_\theta g$ for a particular value of θ is computed entirely from the values of $\widehat{P_\theta g}$ for the same value of θ, so the Fourier data derived from each transmitted signal can be

processed and applied incrementally to the image domain as soon as the reflected signal is received, mixed, and filtered.

This method allows a two-fold parallelization. First, individual radar returns can be processed separately. Secondly, for any angle θ, the values of $\tilde{P}_\theta g(x\cos\theta + y\sin\theta)$ for different points (x, y) can be computed independently of each other, allowing parallelization over the image.

2.3 Reconstruction using spatial filtering — the Wavelet-Based Chirp method

Since the emission and reflection of the signal implement a convolution of the signal with the Radon transform data, it is desirable to use a chirp that implements as much of the reconstruction process as possible. A signal can be produced that preprocesses the return signal and obviates the need to compute $\tilde{P}_\theta g$. We form such a chirp by making use of wavelets, and verify the resulting method analytically and empirically.

With the Wavelet-Based Chirp method, the convolution of $P_\theta g$ with the chirp signal (which we may call the convolving function), an inherent part of the physical system, is no longer a minor nuisance, but the first step in the solution. If the spectral response of the chirp signal equals $|\rho|$, where ρ is the 1-D spectral domain variable, then no interpolation or inverse Fourier transform is required; if $r_\theta(t)$ is the signal returned at angle θ, then $g(x, y)$ is obtained simply by accumulating $r_\theta(x\cos\theta + y\sin\theta)$ at location (x, y), thereby building up $g(x, y)$ as θ varies. In this way, we retain all the advantages of the modified CBP method, and avoid the need to extract and process Fourier data from the return signal. As a bonus, the approximation based on the omission of a quadratic term in the Fourier data extraction (see Munson *et al.*[7]) is eliminated.

We will define a *pseudo-symmetric wavelet* as a function ψ in $L^2(\mathbf{R}^2)$ whose Fourier transform $\hat{\psi}$ is such that the value K_ψ defined by

$$K_\psi = (2\pi)^2 \int_0^\infty \frac{\hat{\psi}(\rho\cos\theta, \rho\sin\theta)}{\rho}\, d\rho \tag{3}$$

is finite and independent of the θ variable. Given a function f in $L^2(\mathbf{R}^2)$ and a wavelet ψ, we define $W_s f(a, b)$, the wavelet transform of f at location (a, b) and scale s, by

$$W_s f(a, b) = (f * \tilde{\psi}_s)(a, b),$$

where

$$\psi_s(x, y) = s\psi(sx, sy)$$

and

$$\tilde{\psi}_s(x, y) = \overline{\psi_s(-x, -y)}.$$

Let us once again assume that $g(x, y)$ is the function to be reconstructed. We will derive a chirp function and a simple reconstruction formula using the chirp. By the wavelet transform inversion formula,[5]

$$g(x, y) = \frac{1}{K_\psi} \int_0^\infty s\,(\psi_s * W_s g)(x, y)\, ds, \tag{4}$$

where K_ψ is given in (3). Writing the convolution on the right side as the inverse Fourier Transform of its own Fourier transform, and using the rules for Fourier transform of a convolution, we find that the right side of (4) is equal to

$$\frac{2\pi}{K_\psi} \int_0^\infty s \int_{-\infty}^\infty \int_{-\infty}^\infty \widehat{\psi_s}(\zeta, \xi)\, \widehat{\tilde{\psi}_s}(\zeta, \xi)\, \hat{g}(\zeta, \xi)\, e^{i(x\zeta + y\xi)}\, d\zeta\, d\xi\, ds$$

$$= \frac{2\pi}{K_\psi} \int_0^\infty s \int_{-\infty}^\infty \int_{-\infty}^\infty |\widehat{\psi_s}(\zeta, \xi)|^2\, \hat{g}(\zeta, \xi)\, e^{i(x\zeta + y\xi)}\, d\zeta\, d\xi\, ds$$

$$= \frac{2\pi}{K_\psi} \int_0^\infty s \int_0^\pi \int_{-\infty}^\infty |\widehat{\psi_s}(\rho\cos\theta, \rho\sin\theta)|^2 \, \hat{g}(\rho\cos\theta, \rho\sin\theta) \, |\rho| \, e^{i\rho(x\cos\theta + y\sin\theta)} \, d\rho \, d\theta \, ds. \tag{5}$$

Let

$$C_{s,\theta}(v) = \frac{1}{\sqrt{2\pi}} \int_{-\infty}^\infty |\widehat{\psi_s}(\rho\cos\theta, \rho\sin\theta)|^2 \, |\rho| e^{i\rho v} \, d\rho,$$

and let

$$C_\theta(v) = \frac{1}{\sqrt{2\pi}} \int_{-\infty}^\infty |\hat{\psi}(\rho\cos\theta, \rho\sin\theta)|^2 \, |\rho| \, e^{i\rho v} \, d\rho.$$

It can be shown by changes of variable that $C_{s,\theta}(v) = C_\theta(sv)$. As we will need $C_{s,\theta}$ and C_θ to be real, it is necessary and sufficient to require that

$$|\hat{\psi}(-\xi, -\zeta)| = |\hat{\psi}(\xi, \zeta)| \tag{6}$$

almost everywhere. Condition (6) holds, for example, if ψ is real or radially symmetric. Clearly,

$$\widehat{C_{s,\theta}}(\rho) = |\widehat{\psi_s}(\rho\cos\theta, \rho\sin\theta)|^2 \, |\rho|.$$

Thus equation (4) is equivalent to

$$g(x,y) = \frac{\sqrt{2\pi}}{K_\psi} \int_0^\infty s \int_0^\pi (P_\theta g * C_{s,\theta})(x\cos\theta + y\sin\theta) \, d\theta \, ds. \tag{7}$$

This formula may be simplified further. Let us suppose that g is wavelet band-limited, by which we mean that there exists $T > 0$ such that for all $s > T, W_s g(a,b) = 0$ for all (a,b). This is conceptually similar to the usual notion of band-limitedness, which is defined in terms of the Fourier transform. Then the integration with respect to s goes only up to T, not up to infinity, allowing a change of order of integration in (7). Integrating with respect to s, using $C_{s,\theta}(u) = C_\theta(su)$, where u is the variable of integration for the convolution, and making the change of variable $w = su$, we find that

$$g(x,y) = \frac{1}{2\pi K_\psi} \int_0^\pi (P_\theta g * h_\theta)(x\cos\theta + y\sin\theta) \, d\theta, \tag{8}$$

where

$$h_\theta(u) = \frac{1}{u^2} \int_0^{uT} w C_\theta(w) dw. \tag{9}$$

It can be shown that $h_\theta(u)$ is continuous at 0, and with proper choice of wavelet it can be made to decay like $1/u^2$.[6] We see that once the convolution has been performed, the only other computation needed to reconstruct g is integration with respect to θ.

Accordingly, we will "chirp" the function $h_\theta(u)$ when viewing the scene from direction θ, and reconstruct the image domain by summing the resulting data over the entire image domain. We note that if the wavelet ψ is radially symmetric, then C_θ and hence h_θ will be independent of θ.

3 DISCUSSION AND ANALYSIS

Our method is analogous to a known method (see Kak[4]) based on the Fourier transform. The usual formula employed by the backprojection algorithm is

$$\frac{1}{2\pi} \int_0^\pi (H'f)(x\cos\theta + y\sin\theta) \, d\theta,$$

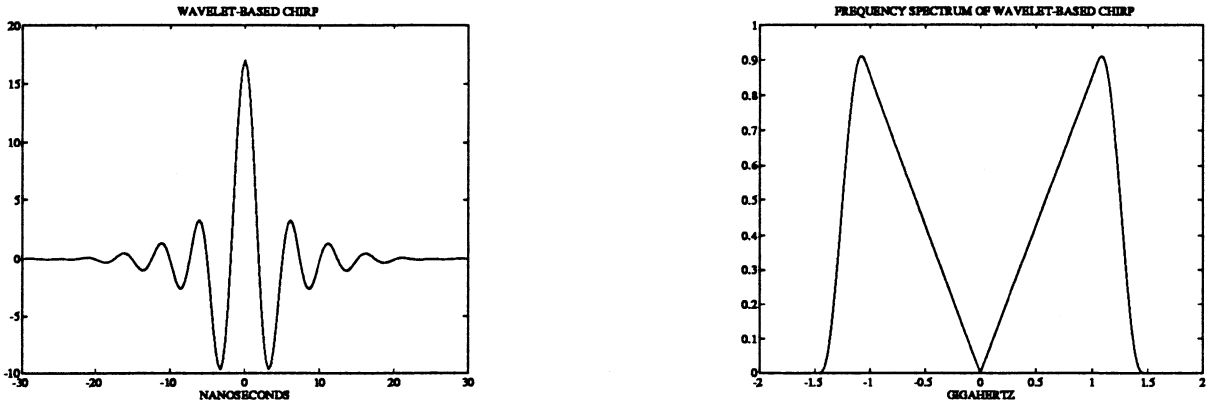

Figure 2: Left, transmitted signal. Right, its frequency spectrum.

where the operator H' denotes differentiation followed by the Hilbert transform. For arbitrary functions, H' cannot be implemented by convolution in the spatial domain, and must be achieved by multiplication by $|\rho|$ in the Fourier domain. However, let us suppose that g is band-limited in the usual sense, namely, that the support of its Fourier transform is contained in a disk of radius R. Then application of H' to g can be achieved by multiplying by $\hat{q}(\rho)$ in the Fourier domain, where $\hat{q}$ is any function that equals $|\rho|$ for $|\rho| < R$. If q is the inverse Fourier transform of $\hat{q}$, then H' can be applied to g by convolving g with q in the spatial domain. Thus

$$g(x,y) = \frac{1}{2\pi} \int_0^\pi (P_\theta g * q)(x\cos\theta + y\sin\theta)d\theta.$$

In fact, if the Fourier transform of the wavelet used to derive the signal in our method vanishes in a neighborhood of the origin, it can be shown[6] that there exists $R > 0$ such that $\hat{h_\theta}(\rho) = |\rho|$ for $|\rho| < R$.

Let us summarize the proposed algorithm:

- We use an appropriate wavelet $\psi(x,y)$ to construct the chirp signal $h_\theta(t)$ for each value of θ.
- Initialize $g(x,y) = 0$ for all (x,y).
- For each available θ in the range of available angles:
  - Chirp the function $h_\theta(t)$ and record the return signal $r_\theta(t)$.
  - For each position (x,y) in the image domain, increment $g(x,y)$ by $r_\theta(x\cos\theta + y\sin\theta)$.

Note that the wavelet approach allows one to chose among many (infinitely many, in fact) different wavelets and use one particularly suited to the task. Empirical investigations will be needed to find the optimal chirp signal.

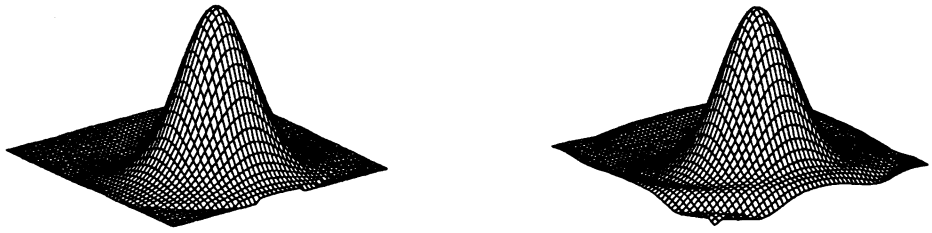

Figure 3: 3-D plots of function f_1, left, and its reconstruction, right.
The reconstruction simulates the wavelet-based chirp method.

4 EXPERIMENTAL DESIGN

4.1 Computation of the signal

Computing $\int_0^{uT} wC_\theta(w)\,dw$ numerically, as suggested by equation (9), is not an effective way of computing h_θ, since computing the integral for relatively large u while keeping the error small would require sampling C_θ at a very large number of points, and accurate computation of the values of C_θ would itself be expensive. Instead, we begin with an analytic expression for $\widehat{C_\theta}(\rho)$, which depends on the choice of the wavelet ψ. We then analytically compute

$$\hat{\phi}(\rho) = \frac{1}{\rho}\frac{d}{d\rho}\hat{C}_\theta(\rho),$$

which is the Fourier transform of $\phi(u) = \int_{-\infty}^{uT} wC_\theta(w)\,dw$. We compute ϕ using a numerical Fourier transform and then use

$$h_\theta(u) = \frac{\phi(u) - \phi(0)}{u^2}. \tag{10}$$

The discrete Fourier transform (DFT) can be modeled as the trapezoidal approximation of the continuous Fourier transform of a function with compact support. Since $\hat{\phi}$ (for our choice of wavelet) is compactly supported, we combine fast (discrete) Fourier transforms with Romberg iteration to compute ϕ to a high degree of accuracy.

Direct evaluation of the right side of equation (10) is not suitable for small values of u, however, because of cancelation error in the numerator. We therefore compute a Taylor series for ϕ centered at zero, which easily provides a Taylor series for h_θ. (There is no x^1 term in the series because ϕ is symmetric as long as the original wavelet satisfies condition (6), and thus its power series only has even exponents.) To compute the series coefficients, we compute the derivatives of increasing order at zero by numerically integrating the compactly supported function $\rho^n\hat{\phi}(\rho)$ for multiple values of n. Errors due to truncation and cancellation are controlled.

The signal $h_\theta(x)$ was derived from a radially symmetric wavelet whose Fourier transform is C^∞ and compactly supported and vanishes in a neighborhood of the origin. The wavelet ψ is defined by $\hat{\psi}(\rho\cos\theta, \rho\sin\theta) = \eta(|\rho|)$, where

$$\eta(\nu) = \begin{cases} \exp\left(\frac{64}{(\nu-40)^2-64}\right) & \text{if } (\nu-40)^2 < 64 \\ 0, & \text{otherwise.} \end{cases}$$

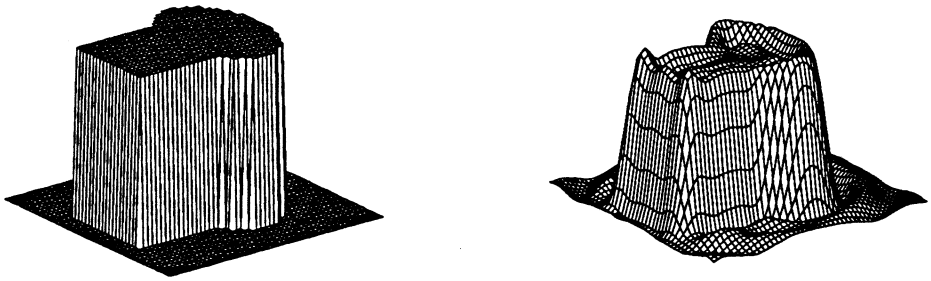

Figure 4: 3-D plots of function f_2, left, and its reconstruction, right.
The reconstruction simulates the wavelet-based chirp method.

The function $h_\theta(x)$ was computed at $x_i = i/100$, where $i = -512, -511, \ldots, 512$. The vector $h_\theta(x_i)$ was padded with zeroes in order to accurately compute the convolution of the chirp signal with the image-domain data, and the DFT of the padded function was computed using an FFT algorithm. The DFT is only used to simulate the spatial domain convolution. Figure 2 displays plots of the resulting signal and its Fourier transform. Note that the duration of the chirp is less than 50 nanoseconds, and that the modal frequency of the chirp is about one Gigahertz.

4.2 Simulation of the return signal

For images defined by mathematical functions, Radon transforms were computed using Simpson's rule and Romberg iteration for 40 viewing angles equally spaced over the range of viewing angles. For each viewing angle, the Radon transform was computed at the same u values for which discrete values of the signal are available, in order to convolve the signal with the Radon transform. As the lines of integration for the Radon transform fell outside the support of the image for large u, this in effect meant that the Radon transform was padded with zeroes. The procedure was the same for grayscale images, except that the Radon transforms were computed exactly, without iteration, by treating each pixel as a square and assuming that the image was constant in that square.

The convolution was effected by multiplying the DFT of the Radon transform, computed by an FFT, by the DFT of the signal, and taking the inverse DFT of the result. Normally, multiplying the DFT's of two vectors is equivalent to the circular convolution of the vectors; since here we need the convolution in the integral sense, not a circular convolution, it was necessary to pad the signal and the Radon transform with zeroes. The result of the convolution was smeared over a 500 by 500 grid.

5 RESULTS

What follows are results of reconstructions using the Wavelet-Based Chirp method. The first function, $f_1(x, y)$, is given by

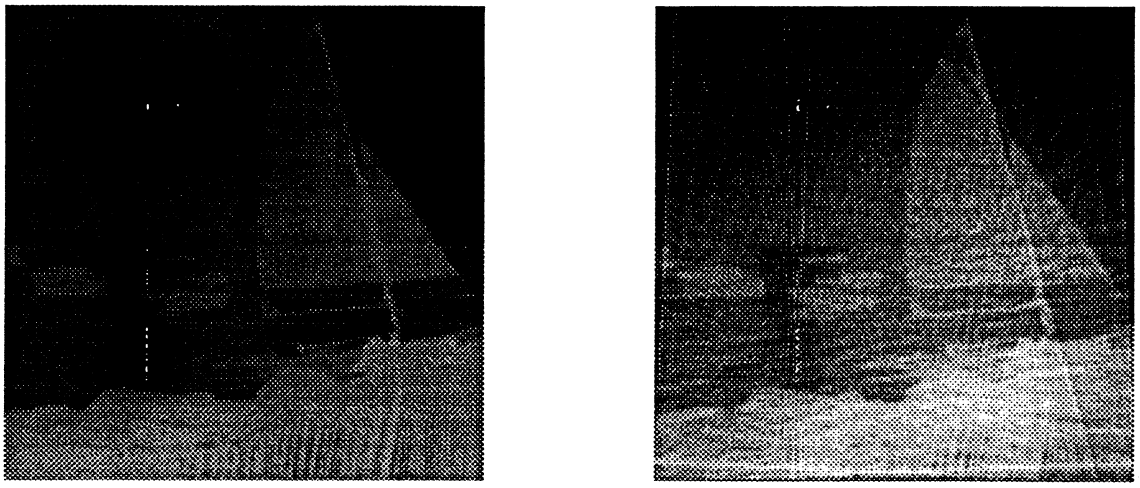

Figure 5: Left, a grayscale image of a boat. Right, its reconstruction.
The boat image is treated as the as the radar reflectivity function. There is an implicit assumption that a given spatial point has a constant reflectivity regardless of the direction of the source radar signal. The reconstruction using forty chirps at equidistant angular samples and refined using a histogram equalization is shown at right. Without the histogram equalization, the image is notably lacking in contrast. This is most probably due to drawbacks inherent in the numerical convolution used in the simulation, and thus images produced using the actual radar signals will not require histogram equalization.

$$f_1(x,y) = \begin{cases} e^{-2(x-1.2)^2-2(y+0.5)^2} + 4e^{-(x+0.1)^2-(y-0.5)^2} - 2e^{-x^2-y^2} & \text{if } \sqrt{x^2+y^2} \leq 2.5 \\ 0 & \text{otherwise} \end{cases}$$

The second function, $f_2(x,y)$, is the characteristic function of the set S in the coordinate plane, where S is the union of the square-shaped open region $-2 < x < 0, -1 < y < 1$ and the ellipse-shaped open region

$$(x-1/2)^2 + \frac{y^2}{(3/2)^2} < 1.$$

Figures 3 and 4 both show a surface plot of one of these functions and its respective reconstruction.

In Figure 5, we see a grayscale image, which is used to model a complicated spatially-varying radar reflectivity function. Assuming that the chirp signal of Figure 2 is used, where the peak frequency is 1 GHz, the size of the image domain is 49 by 49 meters, and the reconstructed image, refined using a histogram equalization, is shown on the right of Figure 5.

6 HEMISPHERE RECONSTRUCTION ALGORITHM

Here, we briefly describe the Hemisphere Reconstruction Algorithm for SPSAR, which is related to the Wavelet-Based Chirp in that both derive from the analogy between SPSAR and computed tomography. It is well known that the conventional SPSAR algorithms are based on the assumption that sets of points on the ground patch equidistant from the radar antenna lie approximately in straight lines, and that this approximation

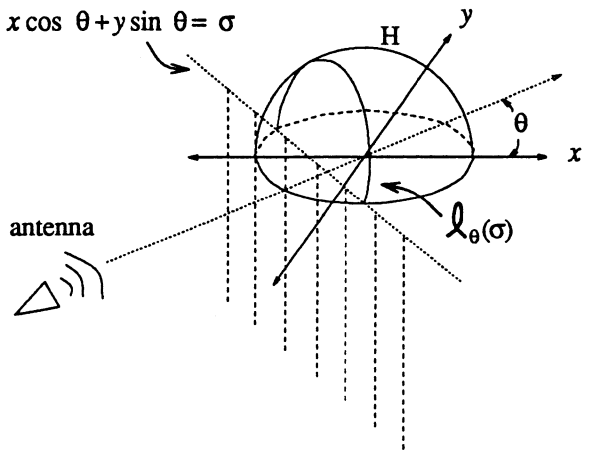

Figure 6: Spherical SAR geometry.
The antenna broadcasts a signal from a point $(-R\cos\theta, -R\sin\theta, 0)$ toward the hemisphere H. The arc $\ell_\theta(\sigma)$ is the set of points on H whose coordinate in the θ direction is σ. It lies in the vertical plane $x\cos\theta + y\sin\theta = \sigma$. Points on $\ell_\theta(\sigma)$ are equidistant from the antenna.

---

leads to limits on the size of the ground patch that may be imaged and on the achievable resolution.[7] Another, more implicit assumption made is that the ground patch lies in a geometric plane. We present here an algorithm that assumes that the ground patch lies on the surface of a hemisphere, and that sets of points on this hemisphere equidistant from the antenna lie on circles (which is geometrically correct).

Let H be the hemisphere given by

$$H = (x, y, z) : x^2 + y^2 + z^2 = 1, z > 0,$$

and let

$$\ell_\theta(\sigma) = (x, y, z) \in H : x\cos\theta + y\sin\theta = \sigma.$$

It is not hard to show that $\ell_\theta(\sigma)$ is a circular arc perpendicular to the x-y plane (see Figure 6). Let us suppose that a radar signal $s(t)$ is emitted by an antenna located at $(-R\cos\theta, -R\sin\theta, 0)$ for some $R > 1$ and some θ. It is not hard to show that the distance $d_A(x, y, z)$ from any point (x, y, z) on H to the antenna is given by

$$d_A(x, y, z) = d_s(x\cos\theta + y\sin\theta),$$

where

$$d_s(\theta) = \sqrt{1 + 2\sigma R + R^2}. \tag{11}$$

It follows from this and the definition of $\ell_\theta(\sigma)$ that all points on $\ell_\theta(\sigma)$ are equidistant from the antenna.

If the radar reflection function g which is to be computed by the SPSAR system is defined on H, then the arcs $\ell_\theta(\sigma)$, for varying θ and σ, will be the curves on which the integral of g will be known.

Specifically, let

$$Q_\theta g(\sigma) = \frac{1}{\sqrt{1-\sigma^2}} \int_{\ell_\theta(\sigma)} g\, dl$$

$$= \int_{-\sqrt{1-\sigma^2}}^{\sqrt{1-\sigma^2}} \frac{g(\sigma\cos\theta - \tau\sin\theta, \sigma\sin\theta + \tau\cos\theta, \sqrt{1-\sigma^2-\tau^2})}{\sqrt{1-\sigma^2-\tau^2}}\, d\tau, \tag{12}$$

where dl in the first integral indicates the arc length integral. These integrals can be extracted by deconvolution from the return signal, since, as we will show in greater detail below,

$$r_\theta(t) = \int_{-1}^{1} Q_\theta g(\sigma)\, s\left(t - \frac{2d_s(\sigma)}{c}\right) d\sigma, \tag{13}$$

where c is the speed of light. (For details on this deconvolution process, see Mann.[6])

To derive Equation 13, we will assume that the radar reflection coefficient is independent of angle of incidence and that the reflection function g vanishes outside a ground patch on the hemisphere. The amplitude of the signal reflected from a point (x, y, z) in the ground patch to the antenna at time t is given by

$$g(x, y, z)\, s\left(t - \frac{2d_A(x, y, z)}{c}\right),$$

where $d_A(x, y, z)$ is the distance of the point (x, y, z) from the antenna. It follows that $r(t)$, the total signal reflected to the antenna from the ground patch at time t, is given by

$$r_\theta(t) = \int_H g(x, y, z)\, s\left(t - \frac{2d_A(x, y, z)}{c}\right) dS,$$

where dS indicates the surface area integral. Since

$$d_A(x, y, z) = d_s(x\cos\theta + y\sin\theta),$$

we may make the following change of variable in order to simplify the last integral:

$$\begin{aligned} \sigma &= x\cos\theta + y\sin\theta \\ \tau &= -x\sin\theta + y\cos\theta \end{aligned}.$$

Then the last integral may be written

$$\begin{aligned} r(t) = \int_{-1}^{1} \int_{-\sqrt{1-\sigma^2}}^{\sqrt{1-\sigma^2}} & g(\sigma\cos\theta - \tau\sin\theta, \sigma\sin\theta + \tau\cos\theta, \sqrt{1-\sigma^2-\tau^2}) \\ & \cdot s\left(t - \frac{2d_s(\sigma)}{c}\right) \frac{d\tau\, d\sigma}{\sqrt{1-\sigma^2-\tau^2}} \\ = \int_{-1}^{1} & Q_\theta g(\sigma)\, s\left(t - \frac{2d_s(\sigma)}{c}\right) d\sigma. \end{aligned}$$

Thus Equation (13) is proved.

We claim next that the $Q_\theta g$ are the Radon transforms $P_\theta \tilde{g}(\sigma)$ of a function $\tilde{g}$ defined in the plane. Specifically, let

$$\tilde{g}(x, y) = \frac{g(x, y, \sqrt{1-x^2-y^2})}{\sqrt{1-x^2-y^2}}, \qquad x^2 + y^2 < 1, \tag{14}$$

and $\tilde{g} = 0$ for $x^2 + y^2 \geq 1$. Using Equation (1) and the definition of $Q_\theta g$ given by (12), it is easy to show that

$$Q_\theta g(\sigma) = P_\theta \tilde{g}(\sigma). \tag{15}$$

Accordingly, since the Radon transform data of $\tilde{g}$ is known, the convolution backprojection algorithm, or any other algorithm for reconstruction from Radon transforms, may be used to compute $\tilde{g}$. Finally, we see from (14) that g is easily reconstructed using the relationship

$$g(x, y, \sqrt{1-x^2-y^2}) = \tilde{g}(x, y)\sqrt{1-x^2-y^2}. \tag{16}$$

6.1 Summary of the algorithm

We have thus derived the following algorithm:

> Let $(-R_1 \cos\theta_1, -R_1 \sin\theta_1, 0), \ldots, (-R_N \cos\theta_N, -R_N \sin\theta_N, 0)$ be the set of points in the x-y-z coordinate system from which radar signals are broadcast. For $i = 1 \ldots N$, broadcast the radar signal and remove the transmitted signal $s(t)$ from the reflected signal $r_\theta(t)$ by deconvolution to obtain $Q_{\theta_i} g(\sigma)$. By (15), this equals $P_{\theta_i} \tilde{g}(\sigma)$.
>
> Reconstruct $\tilde{g}$ from its Radon transforms $P_{\theta_i} \tilde{g}(x)$, using any known algorithm, and finally reconstruct g using
>
> $$g(x, y, \sqrt{1 - x^2 - y^2}) = \tilde{g}(x, y)\sqrt{1 - x^2 - y^2}.$$

We note again that the algorithm is designed for data resident on a sphere, and dispenses with the approximation of regions on spheres by planes which is necessary for conventionaly SAR processing. Also, we note that it is assumed that all antenna positions lie in the x-y plane. While there is a certain degree of latitude in choosing the coordinate system, it must be chosen in such away that the point $(0, 0, 0)$ coincides with the center of the planet. This implies that the antenna path must lie in a plane containing the center of the sphere, or, equivalently, that the points on the planet surface directly below the antenna positions must lie on a single great circle on the planet surface. This great circle may be chosen arbitrarily.

7 ACKNOWLEDGEMENTS

This work forms a portion of the PhD dissertation of Jordan Mann. Research leading to this work was supported in part by AFAL Contract No. F33615-89-C-1089 Work Unit 87-02-PMRE. Thanks to Ed Zelnio, who suggested this line of research.

8 REFERENCES

[1] W.M. Boerner, C.M Ho, and B.Y. Foo, "Use of Radon's projection theory in electromagnetic inverse scattering," *IEEE Transactions on Antennas and Propagation*, vol. AP-29, no. 2, Mar. 1981, pp. 336–341.

[2] M.D. Desai, "A new method of synthetic aperture radar image reconstruction using modified convolution backprojection algorithm," Ph.D. dissertation, Univ. of Illinois, 1985.

[3] M.D. Desai, W.K. Jenkins, "Convolution backprojection image reconstruction for spotlight mode synthetic aperture radar," *IEEE Transactions on Image Processing*, vol. 1, no. 4, Oct. 1992, pp. 505–517.

[4] A. Kak, "Computerized tomography with x-ray, emission, and ultrasound sources," *Proceedings of the IEEE*, vol. 67, no. 9, Sep. 1979, pp.1245–1272.

[5] S. Mallat, "Multifrequency channel decompositions of images and wavelet models," *IEEE Transactions on Acoustical Signal and Speech Processing*, vol. 37, no. 12, Dec. 1989, pp. 2091–2110.

[6] J. Mann, "Enhanced signal processing techniques for spotlight mode synthetic aperture radar and other inverse reconstruction problems," Ph.D. dissertation, Courant Institute of Mathematical Sciences, New York Univ., 1993.

[7] D.C. Munson, Jr., J.D. O'Brien, W.K. Jenkins, "A tomographic formulation of spotlight-mode synthetic aperture radar," *Proceedings of the IEEE*, vol. 71, no. 8, Aug. 1983, pp. 917–925.